



Effect of tea waste on optical and surface area of magnetic cobalt ferrite (CoFe₂O₄) nanoparticles

Abul Kalam^{a,b}

^aDepartment of Chemistry, Faculty of Science, King Khalid University, Abha 61413, P.O. Box: 9004, Saudi Arabia, Tel. +966 172419482; Fax: +966172418426; email: abul_k33@yahoo.com

^bResearch Center for Advanced Materials Science (RCAMS), King Khalid University, Abha 61413, P.O. Box: 9004, Saudi Arabia

Received 8 November 2019; Accepted 7 March 2021

ABSTRACT

The solid magnetic cobalt ferrite (MCF) nanoparticles prepared with different amounts of tea waste under ultrasound-assisted synthetic method were characterized by X-ray diffraction (XRD), scanning electron microscopy (SEM), energy-dispersive X-ray spectroscopy (SEM), transmission electron microscopy (TEM), high-resolution transmission electron microscopy (HR-TEM), UV-visible (UV-Vis) spectroscopy and Brunauer–Emmett–Teller (BET) method. The XRD data confirm the formation of highly pure MCF nanoparticles. TEM and HR-TEM results predict that the morphology of MCF nanoparticles was changed from spherical to cubic and particle size ranging from 29 to 6.5 nm by increasing the content of tea waste. The surface areas of MCF nanoparticles are also increased from 30.78 to 153.82 m² g⁻¹ by increasing the content of tea waste.

Keywords: Magnetic cobalt ferrite nanoparticles; Ultrasound-assisted synthetic method; Optical properties; Surface area

1. Introduction

The magnetic spinel ferrite is oxides of different metals and represented by general formula AB₂O₄, where A and B are positioned at tetrahedral (A site) and octahedral (B site). In the last three decades, magnetic spinel ferrite (MFe₂O₄) nanoparticles are paying much responsiveness to researchers, because of their distinctive magnetic properties. Most of them are used in multidisciplinary fields such as magnetic resonance imaging, catalysis, adsorption, refrigeration scheme, sensors, electrode materials, drug delivery, magnetic cell separation and storage devices [1–6].

Recently the use of magnetic spinel ferrite nanoparticles in the area of wastewater treatment are achieved tremendous momentum due to their attractive electro optical and sensing properties [7–11]. Since magnetic spinel ferrite nanoparticles also have good adsorption efficiency because of their high surface area and more active sites for interaction, many researchers are working in this research area and using the efficient nanoparticles as the active adsorbents.

Recently, Manikandan et al. [12,13] reported various ferrite nanoparticles for the applications of photocatalyst for the degradation of organic dyes.

Due to high coercivity (H_c), moderate saturation magnetization (M_s), large magnetostrictive coefficient, high mechanical hardness and high chemical stability of cobalt ferrites (CoFe₂O₄), it is considered as most promising magnetic oxides as compared to others. Therefore, it is used in different applications, like a catalyst, hyperthermia dealing, magnetic resonance image and biosensor [14–17].

As far as, artificial chemical dyes are one of the most important pollutants of wastewater because of their high toxicity that is probably growth the toxicity-air in the atmosphere. Organic dyes obtained naturally and prepared by synthetic methods are extensively used in a different types of industries like color photography, pharmaceutical, printing, cosmetics, leather, fabric, paper, plastic and other industries [18]. Most of them are carcinogenic, mutagenic and teratogenic due to the existence of non-degradable

aromatic motifs in their structure which results in undesirable effects on human health, microorganisms and ecological welfare. Hence, the remedy and removal of dyes from wastewater is an essential factor and has generated worldwide concern [19]. For the elimination of dyes from wastewater, various methods such as coagulation, flocculation, ion exchange, precipitation, membrane filtration have been developed [20–22].

Up to now, for the synthesis of cobalt ferrite nanoparticles, many methods, like microwave [4,14], co-precipitation [23], ball milling [24], reverse micelles [25], sol-gel [17,26], pulse laser [27], sonochemical [28], aerosol synthesis [29], polymeric precursor [30], hydrothermal methods [16,31,32], modified solvothermal method [33] and thermal decomposition [34] have been used. Nonetheless, toxic reagents that is usually very harmful to the environment and very costly. It is also importantly observed that sonochemical method is much cheap and also reduces the synthesis time and provides the homogeneous structure of cubic shape with high purity. Keeping these factors in mind, we decide to investigate the use of ultrasound-assisted synthesis of biomass-derived spinel cobalt ferrite nanoparticles. Moreover, the literature survey has been explored that few reports for the single-step synthesis of tea-waste loaded spinel cobalt ferrite nanoparticles have been reported. The bioactive compounds present in tea waste might enhance the functionality of cobalt ferrites.

In this study, we prepared tea-waste loaded magnetic nanoparticles under ultrasonic synthetic method and studied their surface area and optical properties. The ultrasonic synthetic method provides the unique size of magnetic cobalt ferrite nanoparticles and is easy and low-cost procedure. We also used various means of investigations such as scanning electron microscopy (SEM), transmission electron microscopy (TEM), high-resolution transmission electron microscopy (HR-TEM), X-ray diffraction (XRD), energy-dispersive X-ray spectroscopy (EDX), Brunauer–Emmett–Teller (BET) method and UV-visible spectroscopy (UV-Vis) to analyze its physical and chemical properties.

2. Experimental

2.1. Materials

All the reagents such as cobalt chloride [$\text{CoCl}_2 \cdot 6\text{H}_2\text{O}$], ferric chloride [$\text{FeCl}_3 \cdot 6\text{H}_2\text{O}$] and sodium hydroxide [NaOH] were used as received without further purification. Tea waste (10 g) was heated with double distilled water (100 mL) at 80°C for 1 h to remove caffeine, tannin and color and then washed repeatedly with double distilled water to become colorless filtrate and also for removal of all the dust particles. The washed tea waste was dried in an oven at 100°C for 12 h, powdered and put in a storage bottle.

2.2. Synthetic procedure

100 mL of 600 mmol solution of ferric chloride, 100 mL of 300 mmol solution cobalt chloride and 50 mL of 3,000 mmol solution of NaOH were prepared in double-distilled water. In continuous of our previous work [33], in a typical synthesis, 25 mL of 600 mmol ferric

chloride hexahydrate ($\text{FeCl}_3 \cdot 6\text{H}_2\text{O}$) was taken in a conical flask which was accumulated within an ultrasonic cleaner (operating at 20 kHz frequency and 2.5 W cm^{-1} of power). In order to increase the pH of the reaction mixture using a dropper in the presence of ultrasonic waves 25 mL of 300 mmol cobalt chloride hexahydrate ($\text{CoCl}_2 \cdot 6\text{H}_2\text{O}$) was slowly added to the reaction mixture followed by the drop-wise addition of 25 mL of 3,000 mmol NaOH solution. The reacting solution was sealed and ultra-sonicated for another 12 h to receive a black precipitate. To obtain pure CoFe_2O_4 nanoparticles, the black precipitate was centrifuge at 3,000 rpm, washed with double distilled water and acetone to become neutral pH and dried overnight in an oven at 100°C . The prepared product was named as US.

We obtained US-1a, US-1b and US-1c samples by the same procedure but in which 0.5, 1.0 and 1.5 g tea waste were added. After 1 h of ultrasonication, the pH of the solution mixture was increased by drop-wise addition of 25 mL of 3,000 mmol NaOH solution.

2.3. Analysis

The X-ray diffractometer (XRD) (Shimadzu Lab X-6000, Tokyo, Japan) with $\text{Cu-K}\alpha$ radiation ($\lambda = 1.5418 \text{ \AA}$) were recorded in the range of 2θ from 10° to 70° at room temperature to determine phase and crystallites size. The scanning electron microscopy (SEM; Hitachi S-4800, Tokyo, Japan) equipped with an EDX spectrometer was employed for the investigation of the surface morphologies and elements present in the magnetic cobalt ferrite (MCF) nanoparticles. The JEOL-2100F (JEOL, USA) TEM and HR-TEM, operating at 200 kV were used to study the morphology and grain size of MCF nanoparticles. BET surface area analyzer (Model 2000e, Quantachrome, USA) were employed for the investigation of surface area, total pore volume and pore size distribution of the powder samples. The UV-Vis spectroscopy of the materials was conducted by PG UV-Vis double-beam spectrophotometer (wavelength range 250–800 nm). The ultrasonic water bath (Elma Germany; 40 kHz) was used for the synthesis.

3. Results and discussion

3.1. Structural properties

Fig. 1 shows the X-ray diffraction patterns of US, US-1a, US-1b and US-1c samples, respectively. Our results exhibit sharp and broad peaks which shown crystalline nature and match with monophasic spinel cobalt ferrite with face-centered cubic structure (space group Fd-3m , JCPDS card no. 22-1086) [35]. Bragg's law is used to calculate interplanar distance (d_{hkl}). Lattice constant (a) and crystallite size (d) of the samples were calculated from the most intense peak signal (311) by using the Debye–Scherrer formula:

$$d = \frac{0.9\lambda}{\beta \cos \theta} \quad (1)$$

Here, λ represents the wavelength of X-ray ($\text{Cu K}\alpha = 0.154 \text{ nm}$), d represents the size of crystallite (nm), β represents the full-width at half maximum (FWHM) of prominent intense peak measured in radians, and θ is peak

angle [36]. The crystallite sizes of all the MCF nanoparticles loaded tea waste samples were measured by the XRD patterns (Table 1). It was noticed that the crystallite sizes of prepared MCF nanoparticles decreases by increasing the content of tea waste. Due to increasing the tea waste content, the diffraction signals were monotonically shifted towards higher angles. It is clear from the above studies that the quantities of tea waste affect the results of synthesized nanoparticles. It was noticed that there is no specific signal of tea waste; this may be due to low mass of tea waste in the cobalt ferrite which is below the detection limit of XRD.

3.2. Morphological properties

Figs. 2a–d exhibit the morphology of MCF nanoparticles prepared by loading with different amount of tea waste using SEM analysis. It is clear from the figure that all prepared samples display just about spherical shape with homogeneous distribution of nanoparticles which indicating that the content of tea waste has a worthy grain

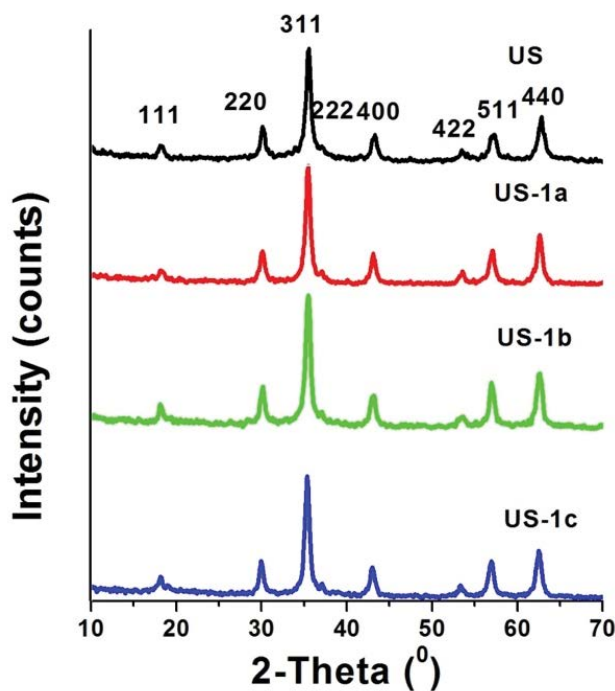


Fig. 1. X-ray diffraction patterns of the samples (US, US-1a, US-1b and US-1c) synthesized by ultrasonic-assisted method at room temperature.

Table 1

X-ray crystallite size, inter-planer spacing, lattice constant and TEM size of tea waste loaded CoFe_2O_4 nanoparticle samples

Sample	Position of 311 peak (°)	Crystallite size (XRD; nm)	Lattice parameter (a; nm)	Interplanar spacing (d_{311} ; nm)	TEM size (nm)
US	35.35403	11.60	0.8410	0.2535	29
US-1a	35.44337	11.38	0.8387	0.2529	11.5
US-1b	35.44488	11.38	0.8387	0.2529	10.5
US-1c	35.44488	11.30	0.8387	0.2529	6.5

growth throughout the synthesis. The average grain size of samples such as US, US-1a, US-1b and US-1c decreases in the range of 25–20 nm by increasing the content of tea waste from 0 to 1.5 g. In the SEM studies the small amount of assemblage could be observed due to the presence of tea waste in ultrasound assisted synthesis.

In addition, the quantification of the samples (US, US-1a, US-1b and US-1c) were determined by EDX analysis (Fig. 3), which confirms that all chemical elements such as Fe, Co, C and O were present in the prepared samples. Thus, it is also established from EDX analysis that tea waste loaded MCF nanoparticles were formed only in one step without calcination and endorse the cleanliness of the samples. Furthermore, by increasing the content of tea waste, the carbon peaks become more intense. The EDX analysis showed that the experimental composition of materials are validated well with the theoretical ratio as shown in Table 2 which corresponds to the formation of monophasic samples.

In addition to this, grain size, morphology and size distribution of tea waste loaded MCF nanoparticles were investigated using TEM and HR-TEM. The relevant TEM micrographs are depicted in Fig. 4 to confirm spherical to cuboidal by increasing the content of tea waste. On increasing the amount of tea waste from 0 to 1.5 g (US, US-1a, US-1b and US-1c) the grain size decreases from 29 to 6.5 nm (Table 1). This result is in good agreement with the result of SEM and XRD. As we know that if the particle size is very small then van der Waals forces support them therefore degree of agglomeration little bit high for all samples. Moreover, the agglomeration is also favor by the magnetic materials [37].

Additionally, the HR-TEM of sample US-1c shown in Fig. 4 which indicates the interplanar spacing around 2.5 Å, corresponding to the (311) crystal plane of MCF nanoparticles.

3.3. Optical properties

The UV-Vis spectra of MCF nanoparticles loaded tea waste are shown in Fig. 5. The following equation is used to calculate the optical band gap (E_g):

$$(Ahv)^n = B(hv - E_g) \quad (2)$$

where $h\nu$ is the photon energy; A represents absorbance, B represents constant related to the material; and n indicates either 2 or $\frac{1}{2}$ for direct transition and

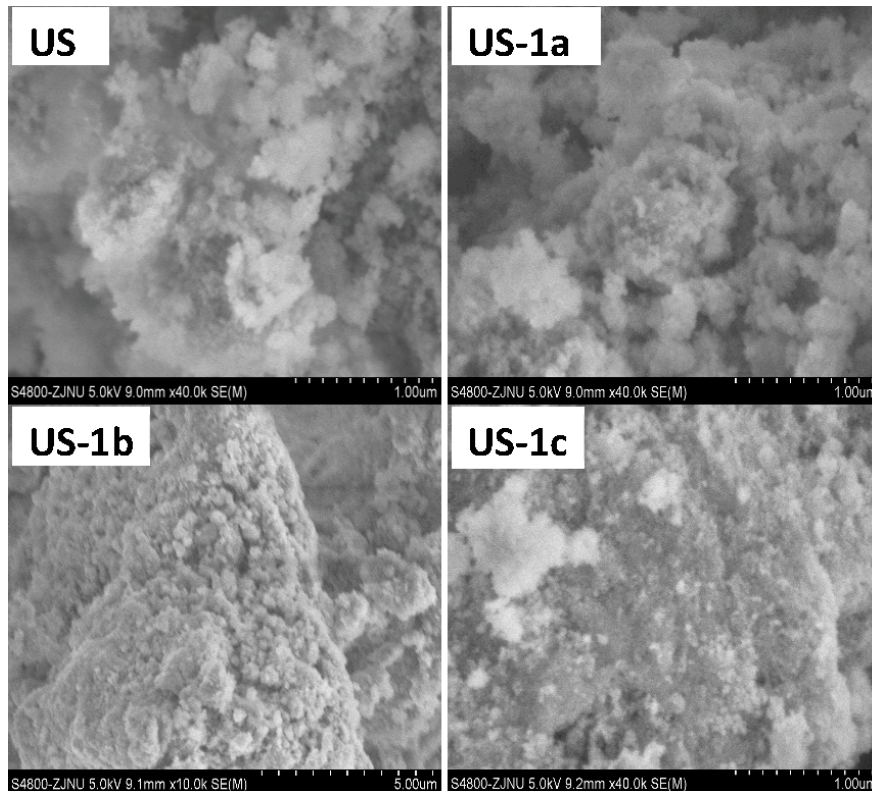


Fig. 2. SEM images of the samples (US, US-1a, US-1b and US-1c) nanoparticles loaded with tea waste.

Table 2
EDX analysis results of metal ratios in the resultant samples

Sample code	Elements	Original ratio	Atomic weight %	Detected ratio
US	Co	$\text{Co}^{2+}/\text{Fe}^{3+} = 0.5$	15.48	$\text{Co}^{2+}/\text{Fe}^{3+} = 0.52$
	Fe		29.28	
US-1a	Co	$\text{Co}^{2+}/\text{Fe}^{3+} = 0.5$	12.75	$\text{Co}^{2+}/\text{Fe}^{3+} = 0.49$
	Fe		25.95	
US-1b	Co	$\text{Co}^{2+}/\text{Fe}^{3+} = 0.5$	10.04	$\text{Co}^{2+}/\text{Fe}^{3+} = 0.54$
	Fe		18.46	
US-1c	Co	$\text{Co}^{2+}/\text{Fe}^{3+} = 0.5$	9.10	$\text{Co}^{2+}/\text{Fe}^{3+} = 0.51$
	Fe		17.81	

indirect transition, respectively [38]. The optical band gaps obtained from absorption peak of samples are presented in insets of Fig. 5, where $h\nu$ at x -axis and $(A/h\nu)^n$ at y -axis [39,40] as shown in insets of Fig. 5. The values of the direct band gap (E_g) were calculated from the curves as 2.5, 2.6, 2.75 and 2.8 eV for US, US-1a, US-1b and US-1c nanomaterials. The results obtained shows that the MCF nanoparticles loaded tea waste cause the high effects on the energy band gap of the synthesized samples. Chen and co-workers have described the optical band gap energy to be 2.38 eV for highly ordered CoFe_2O_4 nanowires array synthesized by modified sol-gel template process and therefore our synthesized tea waste loaded MCF nanoparticles exhibit blue shift [41]. The band gap studies were well associated to the grain size studies as the band gap increases with decreasing the grain size. Due to the decrease

of the crystallite size, the optical band gap energy slightly increases and produces a very weak quantum size effect [42].

3.4. Surface area properties

In general, the skills of adsorbents depend on their surface area. Adsorbents with different features could be obtained by changing of various factors like starting materials, methods, temperature, and time period of reaction etc. Specific surface area, constant, Langmuir surface area, Barrett-Joyner-Halenda (BJH) pore radius, pore volume, Dollimore and Heal (DH) pore radius, Dubinin-Astakhov (DA) pore radius, micro pore volume and Dubinin-Radushkevich (DR) average pore width, micropore surface area of US, US-1a, US-1b and US-1c nanomaterials have

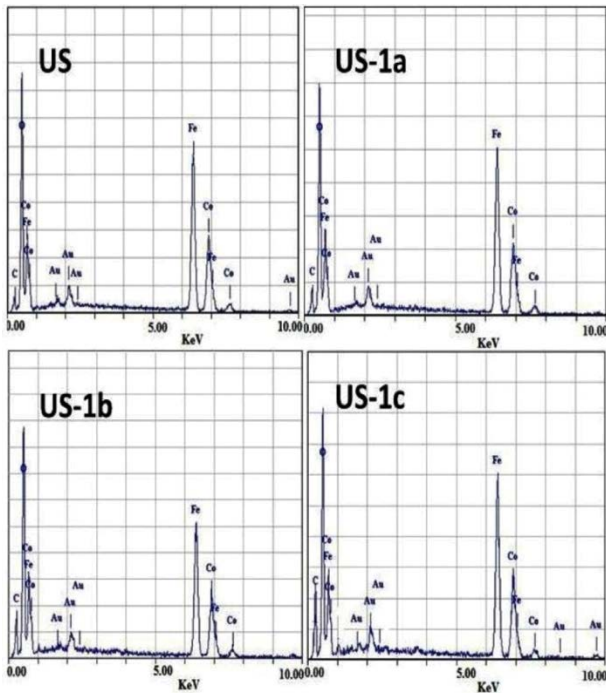


Fig. 3. EDX of the samples (US, US-1a, US-1b and US-1c) nanoparticles loaded with tea waste.

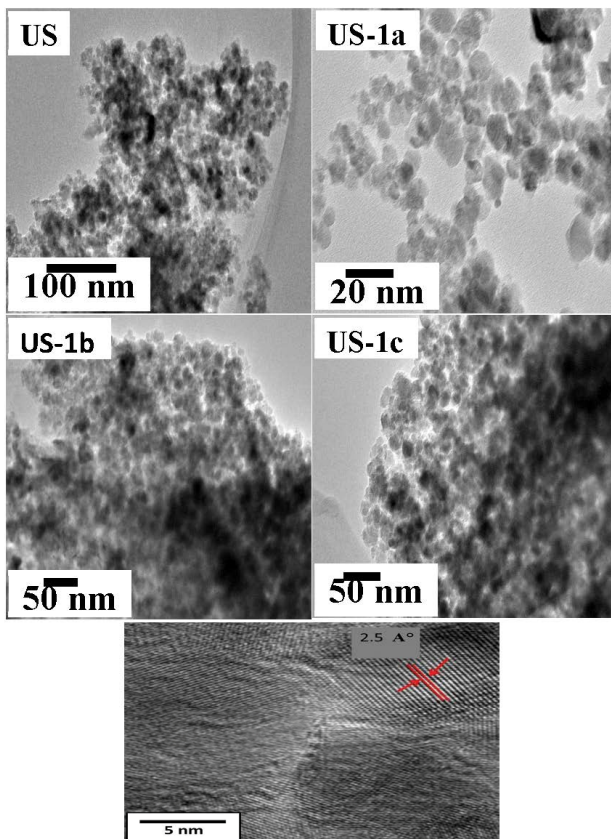


Fig. 4. TEM images of the samples (US, US-1a, US-1b and US-1c) nanoparticles loaded with tea waste and HR-TEM image showing the (311) planes.

been summarized in Table 3. As anticipated, the surface area of US is very small ($30.7 \text{ m}^2 \text{ g}^{-1}$) whereas very large for US-1c ($153.8 \text{ m}^2 \text{ g}^{-1}$), that is higher than CoFe_2O_4 nanoparticles prepared by the co-precipitation method ($17.97 \text{ m}^2 \text{ g}^{-1}$) [43]. We explain from Table 3 that there was an increase in surface area and pore volume of tea waste loaded MCF nanoparticles with increasing of the quantity of tea waste.

The N_2 adsorption–desorption isotherm curves, shown in Fig. 6a, support the calculation regarding the general properties of adsorbents like surface area and pore size exhibiting to IV classification along with H3 type hysteresis. Fig. 6 shows the area of hysteresis loop which depends on P/Po values and increases due to enhancement in surface area of prepared tea waste loaded MCF nanoparticles. The hysteresis loop for samples started from 0.5 (US-1c), 0.6 (US) and 0.7 (US-1a and US-1b) and extended almost to 1. The above mentioned observation reveals that all of the synthesized nanoparticles are in mesoporous nature, which is related to the capillary condensation for filling of the mesopores. The BJH, DH and DA pore size distribution of the synthesized materials are shown in Figs. 6b–d. The result reveals that the quantity of tea waste affects the specific surface area, pore size and pore volume distributions of MCF nanoparticles loaded tea waste materials. Therefore, these materials are applied for adsorption and catalytic properties.

4. Conclusions

To sum up we obtained almost regular and cuboidal spinel structures (6.5–29 nm) of tea waste loaded MCF nanoparticles synthesized through a one pot ultrasonic method at room temperature. The results of EDX and XRD show the high purity of tea waste loaded MCF nanoparticles. The grain size of tea waste loaded MCF nanoparticles was observed by the studies of TEM, SEM and XRD. The results of this study estimate that such tea waste loaded MCF nanoparticles might be an active adsorbent in wastewater treatments and environmental pollution control.

Table 3
BET surface area and pore parameters of (a) US, (b) US-1a, (c) US-1b, (d) US-1c nanoparticles prepared at room temperature

Sample	US-1c	US-1b	US-1a	US
BET surface area ($\text{m}^2 \text{ g}^{-1}$)	153.82	79.02	44.64	30.78
C constant	96.32	65.43	47.43	39.79
BJH pore radius (\AA)	26.13	28.02	26.22	19.59
Pore volume ($\text{cm}^3 \text{ g}^{-1}$)	0.22	0.17	0.10	0.08
DH pore radius (\AA)	28.09	27.87	26.99	19.56
Pore volume ($\text{cm}^3 \text{ g}^{-1}$)	0.21	0.16	0.10	0.09
DA pore radius (\AA)	10.90	14.50	9.90	10.60
Micropore volume ($\text{cm}^3 \text{ g}^{-1}$)	0.15	0.11	0.02	0.01
DR average pore width (\AA)	9.00	11.07	13.30	16.70
Micropore volume ($\text{cm}^3 \text{ g}^{-1}$)	0.05	0.02	0.01	0.01
Micropore surface area ($\text{m}^2 \text{ g}^{-1}$)	161.56	80.85	44.47	32.28

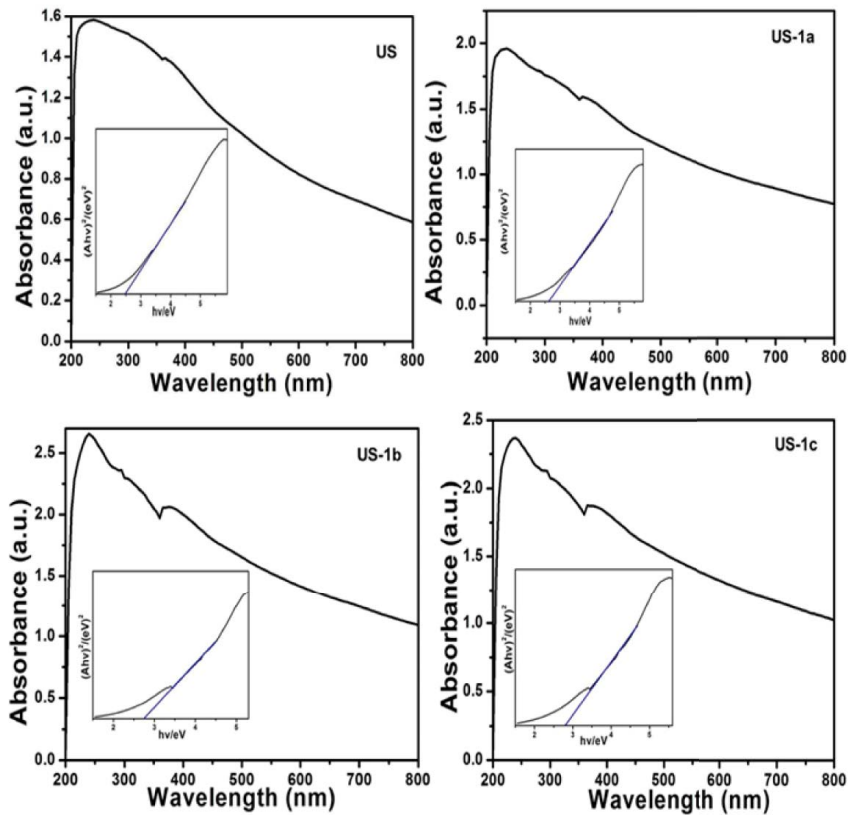


Fig. 5. UV-Vis absorption spectra and plots of $(Ah\nu)^n$ as a function of photon energy ($h\nu$) for the samples (US, US-1a, US-1b and US-1c) nanoparticles loaded with tea waste.

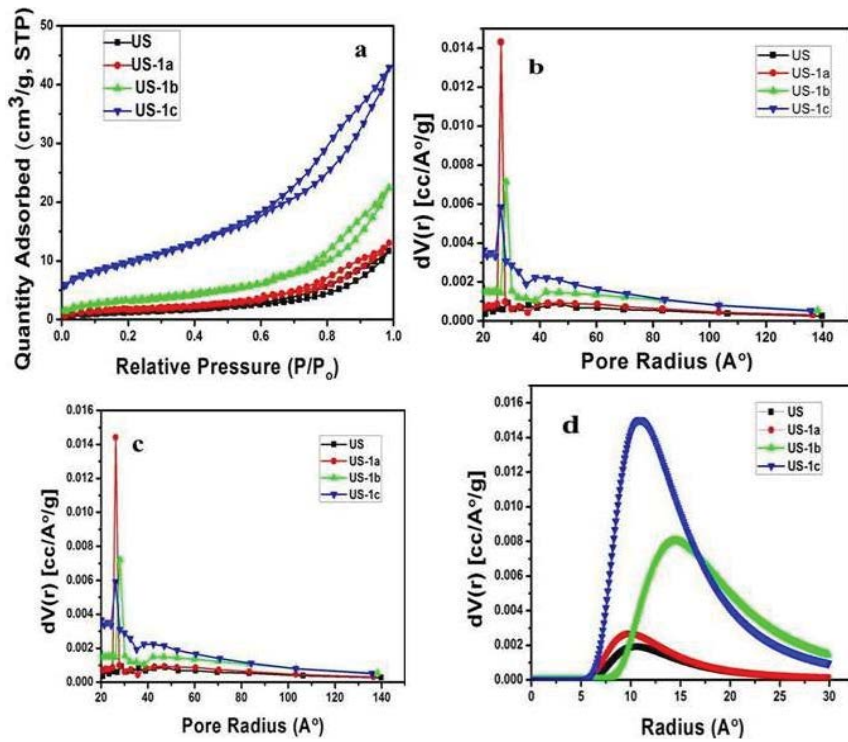


Fig. 6. (a) BET plots, (b) BJH pore size distribution, (c) DH pore size distribution and (d) DA plots of tea waste loaded magnetic cobalt ferrite (CoFe_2O_4) nanoparticles prepared at room temperature.

Acknowledgment

The author (AK) is thankful to the Deanship of Scientific Research at King Khalid University for financial support by grant number R.G.P. 2/86/42. The authors also acknowledge the head of the Department of Physics, King Khalid University, Abha, Kingdom of Saudi Arabia for the XRD and EDX data.

References

- [1] A. Manikandan, R. Sridhar, S.A. Antony, S. Ramakrishna, A simple aloe vera plant-extracted microwave and conventional combustion synthesis: morphological, optical, magnetic and catalytic properties of CoFe_2O_4 nanostructures, *J. Mol. Struct.*, 1076 (2014) 188–200.
- [2] A. Manikandan, M. Durka, K. Seevakan, S.A. Antony, A novel one-pot combustion synthesis and opto-magnetic properties of magnetically separable spinel $\text{MnMg}_{1-x}\text{Fe}_2\text{O}_4$ ($0 \leq x \leq 0.5$) nanophotocatalysts, *J. Supercond. Novel Magn.*, 28 (2015) 1405–1416.
- [3] A.T. Ravichandran, J. Srinivas, R. Karthick, A. Manikandan, A. Baykal, Facile combustion synthesis, structural, morphological, optical and antibacterial studies of $\text{Bi}_{1-x}\text{Al}_x\text{FeO}_3$ ($0.0 \leq x \leq 0.15$) nanoparticles, *Ceram. Int.*, 44 (2018) 13247–13252.
- [4] A. Manikandan, M. Durka, S.A. Antony, A novel synthesis, structural, morphological, and opto-magnetic characterizations of magnetically separable spinel $\text{Co}_x\text{Mn}_{1-x}\text{Fe}_2\text{O}_4$ ($0 \leq x \leq 1$) nano-catalysts, *J. Supercond. Novel Magn.*, 27 (2014) 2841–2857.
- [5] A. Manikandan, M. Durka, M.A. Selvi, S.A. Antony, *Sesamum indicum* plant extracted microwave combustion synthesis and opto-magnetic properties of spinel $\text{Mn}_x\text{Co}_{1-x}\text{Al}_2\text{O}_4$ nano-catalysts, *J. Nanosci. Nanotechnol.*, 16 (2016) 448–456.
- [6] A. Manikandan, M. Durka, S.A. Antony, Magnetically recyclable spinel $\text{Mn}_x\text{Zn}_{1-x}\text{Fe}_2\text{O}_4$ ($0.0 \leq x \leq 0.5$) nano-photocatalysts, *Adv. Sci. Eng. Med.*, 7 (2015) 33–46.
- [7] V.M. Teresita, A. Manikandan, B.A. Josephine, S. Sujatha, S.A. Antony, Electromagnetic properties and humidity-sensing studies of magnetically recoverable $\text{LaMg}_x\text{Fe}_{1-x}\text{O}_{3-\delta}$ perovskites nano-photocatalysts by sol-gel route, *J. Supercond. Novel Magn.*, 29 (2016) 1691–1701.
- [8] B.A. Josephine, A. Manikandan, V.M. Teresita, S.A. Antony, Fundamental study of $\text{LaMg}_x\text{Cr}_{1-x}\text{O}_{3-\delta}$ perovskites nano-photocatalysts: sol-gel synthesis, characterization and humidity sensing, *Korean J. Chem. Eng.*, 33 (2016) 1590–1598.
- [9] A.G. Abraham, A. Manikandan, E. Manikandan, S. Vadivel, S.K. Jaganathan, A. Baykal, P.S. Renganathan, Enhanced magneto-optical and photo-catalytic properties of transition metal cobalt (Co^{2+} ions) doped spinel MgFe_2O_4 ferrite nanocomposites, *J. Magn. Magn. Mater.*, 452 (2018) 380–388.
- [10] A.G. Abraham, A. Manikandan, E. Manikandan, S.K. Jaganathan, A. Baykal, P.S. Renganathan, Enhanced opto-magneto properties of $\text{Ni}_x\text{Mg}_{1-x}\text{Fe}_2\text{O}_4$ ($0.0 \leq x \leq 1.0$) ferrites nanocatalysts, *J. Nanoelectron. Optoelectron.*, 12 (2017) 1326–1333.
- [11] O.K. Mmesele, N. Masunga, A. Kuvarega, T. Ti. Nkambule, B.B. Mamba, K.K. Kefeni, Cobalt ferrite nanoparticles and nanocomposites: photocatalytic, antimicrobial activity and toxicity in water treatment, *Mater. Sci. Semicond. Process.*, 123 (2021) 105523–105540.
- [12] G. Padmapriya, A. Manikandan, V. Krishnasamy, S.K. Jaganathan, S.A. Antony, Spinel $\text{Ni}_x\text{Zn}_{1-x}\text{Fe}_2\text{O}_4$ ($0.0 \leq x \leq 1.0$) nano-photocatalysts: synthesis, characterization and photocatalytic degradation of methylene blue dye, *J. Mol. Struct.*, 1119 (2016) 39–47.
- [13] G. Mathubala, A. Manikandan, S.A. Antony, P. Ramar, Photocatalytic degradation of methylene blue dye and magneto-optical studies of magnetically recyclable spinel $\text{Ni}_x\text{Mn}_{1-x}\text{Fe}_2\text{O}_4$ ($x = 0.0–1.0$) nanoparticles, *J. Mol. Struct.*, 1113 (2016) 79–87.
- [14] E. Hema, A. Manikandan, P. Karthika, S.A. Antony, B.R. Venkatraman, A novel synthesis of Zn^{2+} -doped CoFe_2O_4 spinel nanoparticles: structural, morphological, opto-magnetic and catalytic properties, *J. Supercond. Novel Magn.*, 28 (2015) 2539–2552.
- [15] A. Manikandan, M. Durka, S.A. Antony, Role of Mn^{2+} doping on structural, morphological, and opto-magnetic properties of spinel $\text{Mn}_x\text{Co}_{1-x}\text{Fe}_2\text{O}_4$ ($x = 0.0, 0.1, 0.2, 0.3, 0.4, \text{ and } 0.5$) nanocatalysts, *J. Supercond. Novel Magn.*, 28 (2015) 2047–2058.
- [16] S. Asiri, M. Sertkol, S. Guner, H. Gungunes, K.M. Batoo, T.A. Saleh, H. Sozeri, M.A. Almessiere, A. Manikandan, A. Baykal, Hydrothermal synthesis of $\text{Co}_x\text{Zn}_y\text{Mn}_{1-2y}\text{Fe}_2\text{O}_4$ nanoferrites: magneto-optical investigation, *Ceram. Int.*, 44 (2018) 5751–5759.
- [17] K. Elayakumar, A. Dinesh, A. Manikandan, M. Palanivelu, G. Kavitha, S. Prakash, R.T. Kumar, S.K. Jaganathan, A. Baykal, Structural, morphological, enhanced magnetic properties and antibacterial bio-medical activity of rare earth element (REE) cerium (Ce^{3+}) doped CoFe_2O_4 nanoparticles, *J. Magn. Magn. Mater.*, 476 (2019) 157–165.
- [18] R. Rahimi, H. Kerdari, M. Rabbani, M. Shafiee, Synthesis, characterization and adsorbing properties of hollow $\text{Zn-Fe}_2\text{O}_4$ nanospheres on removal of Congo red from aqueous solution, *Desalination*, 280 (2011) 412–418.
- [19] W. Konicki, D. Sibera, E. Mijowska, Z.L. Bielun, U. Narkiewicz, Equilibrium and kinetic studies on acid dye Acid Red 88 adsorption by magnetic ZnFe_2O_4 spinel ferrite nanoparticles, *J. Colloid Interface Sci.*, 398 (2013) 152–160.
- [20] S. Sultana, Rafiuddin, M.Z. Khan, K. Umar, Synthesis and characterization of copper ferrite nanoparticles doped polyaniline, *J. Alloys Compd.*, 535 (2012) 44–49.
- [21] A.A. Bagade, V.V. Ganbavle, S.V. Mohite, T.D. Dongale, B.B. Sinha, K.Y. Rajpure, Assessment of structural, morphological, magnetic and gas sensing properties of CoFe_2O_4 thin films, *J. Colloid Interface Sci.*, 497 (2017) 181–192.
- [22] A. Kalam, A. Al-Shihri, A.G. Al-Sehemi, N.S. Awwad, G. Du, T. Ahmad, Effect of pH on solvothermal synthesis of $\beta\text{-Ni}(\text{OH})_2$ and NiO nano-architectures: surface area studies, optical properties and adsorption studies, *Superlattices Microstruct.*, 55 (2013) 83–97.
- [23] T. Muthukumar, J. Philip, A facile approach to synthesis of cobalt ferrite nanoparticles with a uniform ultrathin layer of silicon carbide for organic dye removal, *J. Mol. Liq.*, 317 (2020) 114110–114124.
- [24] V. Mahdikhah, A. Ataie, A. Babaei, S. Sheibani, C.W.O. Yang, S.K. Abkenar, Control of structural and magnetic characteristics of cobalt ferrite by post-calcination mechanical milling, *J. Phys. Chem. Solids*, 134 (2019) 286–294.
- [25] C. Singh, S. Jauhar, V. Kumar, J. Singh, S. Singhal, Synthesis of zinc substituted cobalt ferrites via reverse micelle technique involving in situ template formation: a study on their structural, magnetic, optical and catalytic properties, *Mater. Chem. Phys.*, 156 (2015) 188–197.
- [26] C.S. Erhardt, L.E. Caldeira, J. Venturini, S.R. Bragança, C.P. Bergmann, Sucrose as a sol-gel synthesis additive for tuning spinel inversion and improving the magnetic properties of CoFe_2O_4 nanoparticles, *Ceram. Int.*, 46 (2020) 12759–12766.
- [27] M. Oujja, L. Martín-García, E. Rebolgar, A. Quesada, M.A. García, J.F. Fernández, J.F. Marco, J. de la Figuera, M. Castillejo, Effect of wavelength, deposition temperature and substrate type on cobalt ferrite thin films grown by pulsed laser deposition, *Appl. Surf. Sci.*, 452 (2018) 19–31.
- [28] R.S. Yadav, I. Kuřitka, J. Vilcakova, J. Havlica, L. Kalina, P. Urbánek, M. Machovsky, D. Skoda, M. Masar, M. Holek, Sonochemical synthesis of Gd^{3+} doped CoFe_2O_4 spinel ferrite nanoparticles and its physical properties, *Ultrason. Sonochem.*, 40 (2018) 773–783.
- [29] S. Singhal, J. Singh, S.K. Barthwal, K. Chandra, Preparation and characterization of nano size nickel-substituted cobalt ferrites ($\text{Co}_x\text{Ni}_y\text{Fe}_2\text{O}_4$), *J. Solid State Chem.*, 178 (2005) 3183–3189.
- [30] M. Çharagozlu, Synthesis, characterization and influence of calcination temperature on magnetic properties of nanocrystalline spinel Co-ferrite prepared by polymeric precursor method, *J. Alloys Compd.*, 486 (2009) 660–665.
- [31] A.S. Al-Shihri, A. Kalam, A.G. Al-Sehemi, G. Duo, T. Ahmad, One pot synthesis of cobalt ferrites nanoparticles via

- hydrothermal method and their optical studies, *J. Ind. Chem. Soc.*, 91 (2014) 1861–1867.
- [32] S. Das, C. Manoharan, M. Venkateshwarlu, P. Dhamodharan, Structural, optical, morphological and magnetic properties of nickel doped cobalt ferrite nanoparticles synthesized by hydrothermal, *J. Mater. Sci. - Mater. Electron.*, 30 (2019) 19880–19893.
- [33] A. Kalam, A.G. Al-Sehemi, M. Assiri, G. Du, T. Ahmad, I. Ahmad, M. Pannipara, Modified solvothermal synthesis of cobalt ferrite (CoFe_2O_4) magnetic nanoparticles photocatalysts for degradation of methylene blue with H_2O_2 /visible light, *Results Phys.*, 8 (2018) 1046–1053.
- [34] D. Tomar, P. Jeevanandam, Synthesis of cobalt ferrite nanoparticles with different morphologies via thermal decomposition approach and studies on their magnetic properties, *J. Alloys Compd.*, 843 (2020) 155815–155832.
- [35] J. Jiang, L.H. Ai, Synthesis and characterization of Fe-Co binary ferrosinels nanospheres via one-step nonaqueous solution pathway, *Mater. Lett.*, 64 (2010) 945–947.
- [36] M.I. Mendelson, Average grain size in polycrystalline ceramics, *J. Am. Ceram. Soc.*, 52 (1969) 443–446.
- [37] J. Venturini, A.M. Tonelli, T.B. Wermuth, R.Y.S. Zampiva, S. Arcaro, A. Da Cas Viegas, C.P. Bergmann, Excess of cations in the sol-gel synthesis of cobalt ferrite: a pathway to swithching the inversion degree of spinels, *J. Magn. Magn. Mater.*, 482 (2019) 1–8.
- [38] A. Hagfeldt, M. Gratzel, Light-induced redox reactions in nanocrystalline systems, *Chem. Rev.*, 95 (1995) 49–68.
- [39] J.A. Glasscock, P.R.F. Barnes, I.C. Plumb, A. Bendavid, P.J. Martin, Structural, optical and electrical properties of undoped polycrystalline hematite thin film produced using filtered arc deposition, *Thin Solid Films*, 516 (2008) 1716–1724.
- [40] B. Liu, L. Wen, X. Zhao, The structure and photocatalytic studies of N-doped TiO_2 films prepared by radio frequency reactive magnetron sputtering, *Sol. Energy Mater. Sol. Cells*, 92 (2008) 1–10.
- [41] J. Chen, Y. Wang, Y. Deng, Highly ordered CoFe_2O_4 nanowire array prepared via a modified sol-gel template approach and its optical and magnetic properties, *J. Alloys Compd.*, 552 (2013) 65–69.
- [42] N. Kislova, S.S. Srinivasan, Y. Emirov, E.K. Stefanakos, Optical absorption red and blue shifts in ZnFe_2O_4 nanoparticles, *Mater. Sci. Eng., B*, 153 (2008) 70–77.
- [43] Z. Jiao, X. Geng, M. Wu, Y. Jiang, B. Zhao, Preparation of CoFe_2O_4 nanoparticles by spraying co-precipitation and structure characterization, *Colloids Surf., A*, 313 (2008) 31–34.